Computational Investigation on ESIPT-driven Luminescence of Imidazo[1,2-a]pyridine Derivatives Regulated by Inter/Intramolecular Hydrogen bonding

Yasuhiro Shigemitsu[1,2*], Tatsuya Muramatsu[3] and Toshiki Mutai[3]

[1]*Industrial Technology Center of Nagasaki, 2-1303-8, Ikeda, Omura, Nagasaki 856-0026, Japan*

[2]*Graduate School of Engineering, Nagasaki University, 1-14, Bunkyo-machi, Nagasaki 852-8131, Japan*

[3]*Institute of Industrial Science, The University of Tokyo, 4-6-1 Komaba, Meguro-ku, Tokyo 153-8505, Japan.*

E-mail: mutai@iis.u-tokyo.ac.jp

Correspondence should be addressed to Yasuhiro Shigemitsu, shige@tc.nagasaki.go.jp

The three newly synthesized imidazopyridine derivatives bearing inter/intramolecular hydrogen bond were computationally investigated. The quasi stable seven-membered ring systems of the compounds assisted by the intramolecular hydrogen bond exhibit distinct luminescence depending on the surrounding media; in solution, in frozen solution and in solid state. The interesting luminescent properties were studied by means of a series of quantum chemical calculations; i.e., DFT, TDDFT, CASSCF/CASPT2, ADC(2), CC2 and CCSD(T). The stability of the quasi π-conjugated rings was found to be regulated by the delicate balance between intramolecular steric hindrance and intra/intermolecular hydrogen bond strength. The excited state dynamics was explored by the surface hopping trajectory calculations which reproduced the ESIPT process in the first excited singlet state.

Keywords: seven-membered imidazopyridines; ESIPT luminescence; intramolecular hydrogen bond

1. Introduction

A series of luminescent molecules driven by the excited-state intramolecular proton transfer (ESIPT) have attracted much attention from the both viewpoints of the fundamental characteristics and the industrial applications [1][2][3][4]. In solution, representative ESIPT-driven fluorophores exhibit bright emission, such as 2-(2'-hydroxyphenyl)benzimidazole (HPBI)[5][6][7][8], 2-(2'-hydroxyphenyl)benzoxazole (HPBO)[9][10] and 2-(2'-hydroxyphenyl)benzothiazole (HPBT)[11][12]. In solid state, on the other hand, organic luminescence is generally quenched by intermolecular interactions [13]. Nevertheless, modern molecular design and fabrication techniques have realized the enhancement of aggregation-induced emission (AIE) [14][15][16] by suppressing the non-radiative energy dissipation pathways in condensed phases.

An interesting characteristics of ESIPT-driven emission lies in the critical role of intra- [17] and inter- [18] hydrogen bond (HB), which has been investigated experimentally as well as theoretically. One of the representative AIE compounds associated with ESIPT, 2-(2′-hydroxyphenyl)imidazo[1,2-a]-pyridine (HPIP), was initially studied by Douhal et al [19][20]. We have reported the spectroscopic properties of the HPIP and its derivatives, such as the polymorph dependent ESIPT luminescence [21][22], the three-color AIE luminescence [23], and the quantum chemical studies [24][25]. Many of ESIPT-driven HPIP derivatives studied so far hold the intramolecular six-membered ring assisted by the HB upon photoexcitation owing to its structural stability [5][6][7][8][9][10][11][12][26]. A variety of the luminescent ESIPT ring systems have been reported, namely, five-membered [4][27], seven-membered and up to eight-membered[28] ring systems. Since the expansion of the quasi-conjugated ring leads to structural vulnerability, the seven-membered ESIPT system has been rarely reported. For few examples, cis-1-(2-pyrrolyl)-2-(2-quinolyl)-ethane by Tokumaru et al [29], Green Fluorescent Protein (GFP) core chromophore [31] and its derivatives [31] by Chou group were reported, respectively.

From the theoretical standpoint, ESIPT-driven luminescence has been extensively investigated by means of quantum chemical techniques. Prominent computational chemistry groups have focused on several ESIPT compounds and elucidated the luminescence mechanism [17][18][32][33][34][35][36][37][38][39][40][41][42]. Focusing on HPIP, the quantitative MP2 and CC2 quantum chemical studies were reported aiming to find the detailed potential energy surfaces (PES) associated with the ESIPT process [43][44]. Several theoretical models were proposed for understanding the AIE mechanism, such as restriction of intramolecular motion (RIM) [45] via vibronic coupling [46][47] combined with large-scale scheme [48][49], or restricted access to conical intersections

(RACI) [50][51]. To our best knowledge, however, no comprehensive *ab initio* studies have been reported for the luminescence mechanism of seven-membered ESIPT ring systems.

In the present study, the newly reported three seven-membered imidazo[1,2-*a*]pyridine derivatives [52] were computationally investigated. Namely, (8-(2'-hydeoxyphenyl)-imidazopyridine, 8-(3'-hydeoxythienyl)-imidazopyridine, 8-(5'-Fluoro-2'-hydeoxyphenyl)-imidazopyridine,), abbreviated as 8(PhOH)-IP, 8(ThOH)-IP and 8(F-PhOH)-IP, respectively, as shown in Fig. 1., were theoretically investigated by means of a series of quantum chemistry techniques.

The article is organized as follows. Section 2 details the computational strategies and techniques. Section 3 describes the computational analysis of the geometry characteristics, UV/Vis and emission spectra in vacuo, in solution and in solid state, respectively. The ESIPT dynamics in the excited state is discussed by means of the surface hopping calculations. Then, the solid state luminescence switching invoked by intra/intermolecular hydrogen bonding is analyzed and discussed using the dimer model. Concluding remarks are presented in Section 4.

2. Computational Details

The optimized geometries in the ground states were obtained at RI-MP2 level using def2-SV(P) and def2-TZVP basis set. The first excited state geometries were optimized at TDDFT(B3LYP), RI-ADC(2) and RI-CC2 levels, employing the same basis sets used for the ground state geometry. The S_0/S_1 Minimum Energy Conical Intersections (MECIs) were located by means of two state averaged CASSCF(10e,9o)/6-31G(d), including four occupied π−orbitals and one occupied σ−orbital. The vertical transition energies both for UV/Vis and emission were evaluated at TDDFT, RI-ADC(2), RI-CC2, and MS-CASPT2 level, respectively. The MS-CASPT2 singlepoint calculations employed the ten π-orbital active spaces where fourteen active electrons were distributed using ANO-L basis set (MS-CASPT2(14e,10o)/ANO-L). No IPEA shift scheme was employed in the MS-CASPT2 calculations. In solid state, the interaction energies of the hydrogen bonded dimers were computed at RI-CC2/def2-TZVP and RI-CCSD(T)/def2-RZVP level, considering BSSE using counterpoise corrections. RI-MP2, RI-ADC(2), RI-CC2, RI-CCSD(T) and TDDFT calculations were done using TURBOMOLE ver.7.0.1 [53]. The MECI geometry optimizations were carried out using MOLPRO 2015 [54]. The MS-CASPT2 calculations were done using MOLCAS ver.7.8 [55] and openMolcas [56]. Solvent effect was considered by

means of COSMO and PCM scheme, implemented in TURBOMOLE and MOLCAS, respectively. The surface hopping trajectory calculations were dune using Newton-X [57] linked with TURBOMOLE, considering both the S_0 and the S_1 state. The center of energy distribution was set to be the S_0->S_1 vertical excitation energy and the width of energy distribution to be 0.25 eV for the initial condition.

3. Results and Discussion

3.1 Geometrical characteristics of seven-membered ring

The stability of the HB-assisted seven-membered ring is dominated by the delicate balance between its structural deformation and the intra-HB strength as well as the quasi-aromaticity. The crystallographic analysis of the compounds found that 8(ThOH)-IP has almost planarity of the ring with intramolecular-HB (shown in Fig. 2) while 8(F-PhOH)-IP (shown in Fig. 3) has the fairly distorted structure bridged with intermolecular-HB [52]. These experimental findings are contrasted with the GFP-related seven-membered ring [30] [31], which holds the ring almost planarity.

In the ground state of the enol forms (S_0-enol), the optimized key bond length (r_{ON}) and twist angle (ϕ) at the several computational levels are shown in Table 1. 8(PhOH)-IP was correctly optimized with the planar seven-membered ring structure at all the calculation levels. The RI-CC2/TZVP predicted the two key geometries at quantitative accuracy with the O-N distance (2.66 A) and the dihedral angle (40.46 degree) in comparison with the experiment (2.66 Å and 40.58 degree). 8(ThOH)-IP geometries were also correctly optimized at all the calculation levels as in the case of 8(PhOH)-IP with the seven-membered ring kept nearly planar. Interestingly, DFT(B3LYP)/TZVP predicted almost planar structure while RI-ADC(2)/TZVP and RI-CC2/TZVP found the ring slightly distorted. The optimized geometries of 8(F-PhOH)-IP were, in contrast with the other two molecules, inconsistent with the experiment. The compound has the corrupted seven-membered ring with the ring significantly distorted (57.58 degree) and has the intermolecular HB bridge. All the computational methods predicted the less distorted form with the seven-membered ring partially kept (40 degree). This inconsistency between the theory and the experiment is not explainable by a single molecule geometry optimizations and suggests us to consider the competition between intra- and intermolecular HB. This issue is discussed in the following section.

In the first excited state of enol-form (S_1-enol) and keto-form (S_1-keto), the computed geometrical parameters are shown in Table S1 and S2. For 8(PhOH)-IP, the optimized geometries of S_1-enol were exclusively obtained at RI-ADC(2)/TZVP and RI-CC2/TZVP levels respectively, and other computational methods failed to locate the stable S_1-enol structure and the geometries slipped into the S_1-keto form. Interestingly, TDDFT(B3LYP) predicted the fictitious S_1-keto structure with the two moieties being nearly perpendicularly distorted. The hindered geometry has the proximity with the corresponding S_0/S_1-MECI rather than the moderately twisted S_1-keto local minimum. RI-ADC(2) and RI-CC2, on the other hand, correctly located the modestly twisted S_1-keto minimum.

For 8(ThOH)-IP, all the computational schemes successfully located the S_1-enol stable structures in contrast with the cases of 8(PhOH)-IP. TDDFT(B3LYP)/TZVP predicted the moderately twisted form while RI-ADC(2)/TZVP predicted the slightly twisted form in comparison with ones in the ground state, respectively. RI-CC2/TZVP predicted almost planar S_1-enol form. It is notable that RI-ADC(2)/TZVP and RI-CC2/TZVP predicted the shorter intramolecular O-H distance by ca. 0.1 A for the S_1-enol than for the S_0-enol, which indicates the compact seven-membered ring structure is maintained in the S_1-enol. For the S_1-keto form, TDDFT(B3LYP)/TZVP predicted the planar form similar to the one in the S_0-enol while RI-ADC(2)/TZVP and RI-CC2/TZVP predicted the more distorted form than the one in the S_0-enol. The structural differences between TDDFT and RI-ADC(2)/RI-CC2 are also reflected on the O-N distance which was computed to be slightly longer by 0.03 Å than the one in the S_0-enol using TDDFT while significantly longer by ca. 0.2 Å than the one using RI-ADC(2)/RI-CC2.

For 8(F-PhOH)-IP, only RI-ADC(2)/TZVP successfully located the S_1-enol structure. The other methods failed and slipped into the S_1-keto form. The RI-ADC(2)/TZVP structure is less distorted than the one in the S_0-enol. For the S_1-keto form, TDDFT(B3LYP)/TZVP optimized structure slipped into the perpendicularly distorted one in proximity to the S_0/S_1-MECI while the optimized structures computed by RI-ADC(2)/TZVP and RI-CC2/TZVP successfully reached the S_1-keto local minimum. The different results between TDDFT and RI-ADC(2)/RI-CC2, which was also found in the case of 8(PhOH)-IP, can be attributed to the well-known B3LYP failure to correctly describe the intramolecular charge transfer character of twisted molecules.

Further analysis of the seven-membered ring structure was done from aromaticity viewpoint. That is, HOMA (Harmonic Oscillator Model of Aromaticity) analysis [58] was carried out, as shown in Table 2. The original HOMA formula is shown below.

$$HOMA = 1 - \frac{1}{n}\sum_{i}^{n} \alpha_i (R_{o,i} - R_i)^2$$

Where, n is number of bonds, parameter α_i and the reference bond length $R_{o,i}$ of C-C, C-O and C-N were used ones in the reference [59]; $\alpha_{CO} = 157.38$, $\alpha_{CN} = 93.52$, $\alpha_{CC} = 257.7$, $R_{o,CO} = 1.265$, $R_{o,CN} = 1.334$, $R_{o,CC} = 1.338$. We employed the quasi-HOMA expression [17] which exclusively considers the five-membered moiety (n=5) by ignoring the two HB (N-H and O-H). 8(ThOH)-IP showed the largest index value among the three compound owing to the strong π-conjugation nature in planar structure. The gap between 8(PhOH)-IP and 8(F-PhOH)-IP (in-plane form) is negligibly small with small variation between the two compounds despite the enhanced F-H repulsion in 8(F-PhOH)-IP. On the other hand, the index of 8(F-PhOH)-IP (in-plane form) with the seven-membered ring is larger than 8(F-PhOH)-IP (out-of-plane form bridged by intermolecular HB), reflecting the aromaticity corruption of the one out-of-plane form. The quasi-HOMA indexes of the six-membered HPIP rings were reported by Stasyuk et al [17], which is ca. 0.4, to be larger than those of 8(PhOH)-IP and 8(F-PhOH)-IP. This indicates that the six-membered ring is optimal size to form the stable ESIPT ring with the smaller bond alternation than the hindered seven-membered ring.

3.2 Vertical transition energy : absorption and emission

In cyclohexane and in frozen methytetrahydrofran, 8(PhOH)-IP and 8(F-PhOH)-IP exhibit dual emission maxima, i.e., the intense “blue” peak derived from the S_1-enol and the weak “red” ESIPT one. 8(ThOH)-IP, meanwhile, shows the solo “red” peak. In protic methytetrahydrofran, all the three compounds show solo “blue” peak. This is because protic solvent can form solute-solvent complex bridged by intermolecular HB and hinder intramolecular seven-membered ring formation. This is known as Douhal’s hypothesis on the role of aprotic solvent in the emission properties of ESIPT compounds [19][20][60].

First, the calculated vertical transition energies of 8(PhOH)-IP are shown in Table 3. The shape of emission spectra depend on the surrounding media (solvent, in solution /solid), as shown in Fig. 4. On the intense absorption peak (3.79 eV observed in cyclohexane), RI-CC2/TZVP offered the best theory-experiment agreement with 0.19 eV gap among the computations. TDDFT underestimated the energy by ca. 0.2eV while RI-ADC(2)/SVP and RI-CC2/SVP overestimated that by ca. 0.3 eV. The

highly accurate MS-CASPT2(14e,10o)/ANO-L overestimated the energy by 0.27 eV. The solvent effects on the peak positions are not critical with the shift of 0-0.06 eV from the ones calculated in vacuo. On the S_1-enol, the optimized geometries were carefully and laboriously obtained at RI-ADC(2)/TZVP and RI-CC2/TZVP levels through the repeated partial optimizations of the enol O-H distance and all the other geometrical parameters alternately. The geometry optimizations other than at RI-ADC(2)/TZVP and RI-CC2/TZVP levels failed to locate the local minima in the S_1-enol form and the geometry directly reached the S_1-keto form. This indicates that the energy minimum in the S_1-enol is quite shallow and strongly dependent on the computational strategies. On the emission peak from the S_1-enol form (3.32 eV in cyclohexane), TDDFT calculations underestimated the energy by ca. 0.4 eV and RI-ADC(2)/RI-CC2 by ca. 0.1-0.2 eV, respectively. The best theory-experiment agreement was obtained by using MS-CASPT2(14e,10o)/ANO-L combined with COSMO solvent scheme, with the gap of 0.005 eV. On the emission peak from the S_1-keto (2.11 eV in cyclohexane), TDDFT(B3LYP)/SVP failed to find the optimized structure due to the wavefunction instability at the S_0/S_1 proximity. RI-ADC(2) and RI-CC2 calculations successfully located the twisted S_1-keto form and underestimated the energy by ca. 0.1-0.6 eV. These results imply that the optimized structure of the twisted S_1-keto is close to that of the S_0/S_1-MECI.

Next, the calculated vertical transition energies of 8(ThOH)-IP are shown in Table S3. On the absorption band energies (3.47 eV in cyclohexane), the compact calculations TDDFT(B3LYP)/SVP and TD(B3LYP)/TZVP showed excellent performance with the theory-experiment agreements within 0.1 eV. RI-ADC(2) and RI-CC2 results overestimated the gap by 0.4 eV (SVP) and 0.2 eV(TZVP), respectively. MS-CASPT2(14e,10o)/ANO-L including solvent effect overestimated the energy by 0.31 eV. The results showed the equivalent prediction accuracies of TDDFT, RI-ADC(2) and RI-CC2 with the most elaborating MS-CASPT2/ANO-L. On the emission peak from S_1-enol (3.16 eV in cyclohexane), all the calculations overestimated the energy with the gap of ca. 0.1-0.4 eV other than MS-CASPT2(14e,10o)/ANO-L combined with COSMO. On the emission peak from the S_1-keto (2.63 eV in cyclohexane), the two TDDFT calculations considerably overestimated the energy by nearly 1 eV while the RI-ADC(2)/SVP and RI-ADC(2)/TZVP calculations offered the good agreements within the gap of ca. 0.1 eV. MS-CASPT2(14e,10o) combined with COSMO gave the excellent agreement with the 0.03 eV gap.

Finally, the calculated vertical transition energies of 8(F-PhOH)-IP are shown in Table S4. For the absorption peak (3.92 eV in methyltetrahydrofuran), the two TDDFT results underestimated the energy by ca. 0.2-0.3 eV. Conversely, RI-ADC(2) and RI-CC2 consistently overestimated the energy by ca. 0.2-0.3 eV. The best agreement was obtained by using MS-CASPT(14e,10o) combined with COSMO with the gap of 0.19 eV. For the emission peak from the S_1-enol (3.22 eV in cyclohexane), the fully optimized geometry, which was solely obtained by using RI-ADC(2)/TZVP, was employed for all the singlepoint spectral calculations. For the emission peak from S_1-keto (2.07 eV in cyclohexane), as in the case of 8(PhOH)-IP, TDDFT(B3LYP)/SVP calculation gave the significantly small energy, of which structure presumably corresponds to the S_0/S_1-MECI. The best agreement was obtained by using the MS-CASPT(14e,10o) combined with COSMO with the gap of 0.06 eV.

The simulated absorption and emission spectra along with the experimental ones of 8(PhOH)-IP in cyclohexane solution are show in Fig. S1. The simulated spectra were constructed from the calculated peaks at MS-CASPT2(14e,10o)/ANO-L level by means of Lorentzian interpolation of which parameters were iteratively optimized. The calculated peak position of the absorption spectrum shifted into the shorter wavelength region than the experimental one. The calculated first peak position of the emission spectra shifted into the shorter wavelength region as well. The relative peak height of the first and the second emission peaks was reversed in the simulated emission spectra. These inconsistencies between the theory and the experiment may be derived from some computational limitations. For example, the MS-CASPT2(14e,10o) includes only π–π^* orbitals due to the huge computational burden which lack the contributiosn from the σ–π^* electron correlations. The solvent effect calculation (PCPM) is based on the continuum approximation which does not consider the explicit interaction between the solute and the solvent.

Both the S_1-keto and the S_1-enol states of the three molecules consistently have the overwhelmingly large HOMO->LUMO configurations as shown in Table S5. Upon the S_0->S_1 excitation associated with ESIPT, the significant π–π^* charge transfer takes place from the phenol moiety to the imidazopyridine moiety, as shown by the corresponding HOMOs and LUMOs in Fig.S2.

3.3 PES exploration and luminescence mechanism

The PESs along ESIPT pathways of the three compounds were computationally analysed. It is noteworthy that the PES landscape is heavily dependent on the computational methods. The most extensive RI-CC2/TZVP gave the rigorous PES, while other calculation schemes (TDDFT, RI-ADC(2) and RI-CC2/SVP) gave the untrustworthy results.

First, 8(PhOH)-IP PES was examined with the energy diagram at key geometries; S_0-enol, S_1-enol, S_1-keto and S_0/S_1-MECI, as shown in Fig.5. Upon the S_0->S_1 vertical excitation, the two relaxation pathways exist from the Franck-Condon (FC) state; one relaxes into the S_1-enol form and the other into the S_1-keto form which is further accessible to the S_0/S_1-MECI by using the excess energy at the FC state. The computational results indicate that the one emission peak is originated from the S_1-enol and the other peak from the S_1-keto, respectively. The S_1-keto, however, can radiationlessly go back to the ground state via the S_0/S_1-MECI depending on the energy gap between the S_1-keto and the S_0/S_1-MECI. This theoretical speculation is consistent with the experimental results in cyclohexane solution, where the dual emission peaks are observed at 3.32 and 2.11 eV corresponding to the S_1-enol and the S_1-keto luminescence, respectively. The dual emission peaks indicate that the two emission are competitive in spite of the presence of the keto-S_0/S_1-MECI. On the other hand, no ESIPT emission was observed in protic methytetrahydrofran or in crystalline state. In solid state, the relaxation pathway via the S_0/S_1-MECI is hampered by the steric hindrance and the solo emission peak is observed from the more stable S_1-keto than the S_1-enol, which is consistent with the experiment. The S_0 and S_1 PES of 8(PhOH)-IP connecting the planar S_1 state and the S_0/S_1-MECI varying the twist angle from 0 to 90 degrees are shown in Fig. 6. The energy gap (0.011 a.u.) remains at the S_0/S_1-MECI because the MECI geometry was optimized by CASSCF(10e,9o)/6-31G(d), not by RI-CC2/TZVP. This discrepancy is expected to diminish by means of the MECI exploration consistently at RI-CC2 level calculation [41][42]

Next, For 8(ThOH)-IP, the two relaxation pathways from the FC state are connected to the S_1-enol and the S_1-keto in a similar situation to 8(PhOH)-IP, as shown in Fig. S3. The S_1-keto is more stable than the S_1-enol. In solution, the FC state traces the two decay pathways in a competitive manner where the S_1-keto can further reach the S_0/S_1-MECI with the small energy gap of 0.06 eV between the S_1-keto and the S_0/S_1-MECI. As a result, the solo emission originated from the S_1-enol is expected to be observed,

which is consistent with the experiment. In solid, the inaccessibility to the S_0/S_1-MECI of the S_1-keto due to the intermolecular hindrance leads to the solo emission originated from the stable S_1-keto, which is also consistent with the experiment.

Finally, for 8(F-PhOH)-IP, the relative energy levels of the S_1-enol and S_1-keto is similar to the two molecules abovemensioned. The S_1-keto is more stable than the S_1-enol, as shown in Fig. S4. In solution, the dual emission is expected to be observed as explained in the case of 8(PhOH)-IP, which is consistent with the dual emission both from the S_1-keto and the S_1-enol observed in cyclohexane. In solid, as in the case of the two other compounds, the solo ESIPT emission from the S_1-keto is predicted as a result of inaccessibility to the S_0/S_1-MECI. The experimental solo peak, however, is derived from the S_1-enol, not from the S_1-keto. This critical inconsistency is the theoretical limitation based on the isolated molecule model at present. As explained in the next chapter using the dimer model, the intermolecular HB dominantly stabilizes the S_1-enol and the S_1-keto is not generated in solid state. The emission, therefore, is not originated from S_1-keto but from S_1-enol which is generated by the intermolecular HB.

A typical surface hopping trajectory of 8(PhOH)-IP starting from the FC state at TDDFT(B3LYP)/SVP is illusrated in Fig.7. The trajectory switch from the S_1-enol and the S_1-enol keto occurred at 17 fs associated with ESIPT, which reflects that the PES along ESIPT is barrierless without any local minimum in the S_1-enol at TDDFT(B3LYP)/SVP level. Around 50 fs, the energy gap between the two states becomes sufficiently small (0.02 a.u.) which corresponds to the S_0/S_1 MECI.

3.4 Role of Intra- and inter- hydrogen bond in solid state emission

In solid state, 8(PhOH)-IP and 8(ThOH)-IP show the ESIPT emission originated from the S_1-keto while 8(F-PhOH)-IP shows the S_1-enol emission. The single molecule calculations in the previous section predicted that all the three compounds are expected to show ESIPT emission in solid state because the S_1-FC state stays at the S_1-keto due to the inaccessibility to the S_0/S_1-MECI, in contrast to the situation in solution. This theoretical conclusion, however, is inconsistent with the S_1-enol emission of 8(F-PhOH)-IP.

To understand this emission anomaly of 8(F-PhOH)-IP, the enol dimer of 8(F-PhOH)-IP bridged by intermolecular HB was computationally examined. First, the enol monomer with the in-plane-HB and the

out-of-plane-HB were fully optimized at RI-CC2/TZVP levels, respectively. Then the energies were evaluated further by RI-CCSD(T)/TZVP singlepoint calculations. The intermolecular HB energy of 8(F-PhOH)-IP was evaluated as the gap between the sum of the two isolated out-of-plane S_0-enol monomers and the intermolecular-HB-bridged dimer at crystallographic geometry (E_1=0.034 a.u.). Alternatively, the BSSE-corrected HB energy for the HB-bridged dimer was evaluated considering counterpoise correction (E_2=0.029 a.u.). In turn, the BSSE contribution to the HB energy was proved to be (E_1)-(E_2)=0.005 a.u.

The value of BBSE-corrected HB energy (E_2) was hypothetically applied to 8(PhOH)-IP and 8(ThOH)-IP. This is because (E_2) cannot be computationally evaluated, since no HB-bridged dimer for the two molecules were experimentally obtained.

Fig.8 shows the relative energy diagram of the monomer (in-plane), the monomer (out-of-plane) and the dimer (intermolecular HB-bridged) of 8(F-PhOH)-IP. The results illustrate that the HB-bridged dimer is more stable by 0.14(0.19) eV than the two independent monomers (in-plane). In case of 8(ThOH)-IP, the two independent monomers (in-plane) is more stable by 0.35(0.25) eV than the dimer. These results are consistent with the experiments, where 8(F-PhOH)-IP shows the enol emission while 8(ThOH)-IP shows ESIPT luminescence. In case of 8(PhOH)-IP, the HB-bridged dimer is slightly favourable than the two independent monomer (in-plane) by as small as 0.08(0.14) eV, which is comparable to the BSSE error. This result contradicts with the ESIPT emission of 8(PhOH)-IP. This is because the hypothetical bridged dimer structure of 8(PhOH)-IP may be different from the experimental one of 8(F-PhOH)-IP. The intermolecular HB energy of 8(PhOH)-IP, in turn, may be different from (E_2=0.029 a.u.) and be smaller than that of the optimized structure. This speculation leads to the ESIPT emission, not the enol emission of 8(PhOH)-IP in solid state. In addition, the complicated crystal field effect beyond dimer interactions may decisively regulates the emission turning of 8(PhOH)-IP, which will be able to be computationally treated with QM/MM or other sophisticated large scale computational methods in future.

4. Concluding Remarks

The geometries, absorption and luminescence properties of the new three imidazo[1,2-a]pyridine derivatives were computationally investigated by means of DFT, TDDFT, ADC2, CC2, CCSD, CCSD(T) and MS-CASTP2 quantum chemistry calculations. Experimentally, the three compounds 8(PhOH)-IP, 8(ThOH)-IP and 8(F-PhOH)-IP exhibit the distinctive luminescence behaviour which is originated from the sterically hindered seven-membered ring assisted by inter/intramolecular HB in solution and in solid state. The geometrical characterises of the strained conjugation structures were computationally evaluated both in the ground and the lowest excited states. The S_1-enol forms of 8(PhOH)-IP and 8(F-PhOH)-IP failed to reach the optimized structures by the several QM methods, where TDDFT failed to locate the S_1-keto local minima and the S_1 Franck-Condon structures fallen into the S_0/S_1-MECI fictitiously. The quasi-HOMA analysis successfully illustrated the aromaticity differences among the three compounds, which are mainly originated from the C-C bond alternation magnitude in the intramolecular conjugation systems. The absorption maxima in solution were quantitatively reproduced by the series of calculations but the absolute agreements with the experiment were obtained by method-by-method. The highly accurate RI-CC2/TZVP did not necessarily give the best theory-experiment agreement. The competitive emission maxima derived from the two S_1-forms (the S_1-enol and the S_1-keto) were computationally evaluated both in solution and solid state. In solution, the intense emission band was assigned to the S_1-enol associated with the weak band of the S_1-keto, because the S_1-keto readily reaches the S_0/S_1-MECI and deactivates nonradiatively. In solid state, the non-radiative ultrafast pathway via the S_0/S_1-MECI is blocked by the aggregation effect. The solid state luminescence from the S_1-keto, therefore, is mainly observed associated with ESIPT. The exception to this scenario is 8(F-PhOH)-IP which shows the S_1-enol emission, not the ESIPT emission. This anomaly was successfully explained by considering the intermolecularly HB-bridged dimer models, where the inter-HB dimer (enol emission) is stable than the intra-HB dimer (ESIPT emission) specifically in case of 8(F-PhOH)-IP. The computed BSSE-corrected HB energies indicated that the switching between the enol/ESIPT emission in solid state is governed by the delicate balance between inter- and intra-HB strength. The turning point lies at between 8(PhOH)-IP (the key twist angle is 40.58degree) and 8(F-PhOH)-IP (57.58degree), which separates the enol/ESIPT emission derived from inter-/ intra- HB structures.

Acknowledgement

The author (Y.S.) and (T.M.) was financially supported by Grant-in-Aids for Scientific Research (C) (15K05434)

and (16K05743/19K05434) from Japan Society for the Promotion of Science, respectively.

Conflicts of interest

The authors have no conflict of interest to declare.

References

[1] J. Zhao, S. Ji, Y. Chen, H. Guo, P. Yang, Excited state intramolecular proton transfer (ESIPT): from principal photophysics to the development of new chromophores and applications in fluorescent molecular probes and luminescent materials, Phys. Chem. Chem. Phys. 14 (2012) 8803-8817.
[2] J.E.Kwon and S.Y.Park, Advanced Organic Optoelectronic Materials: Harnessing Excited-State Intramolecular Proton Transfer (ESIPT) Process, Adv.Mater. 23 (2011) 3615-3642.
[3] J.Wu, W.Liu, J.Ge,H.Zhang and P.Wang, New sensing mechanisms for design of fluorescent chemosensors emerging in recent years, Chem.Soc.Rev. 40 (2011) 3483-3495.
[4] A.P.Demchenko, K.-C.Tang and P.-T.Chou, Excited-state proton coupled charge transfer modulated by molecular structure and media polarization, Chem.Soc.Rev. 42 (2013) 1379-408.
[5] K. Benelhadj, J. Massue, P. Retailleau, G. Ulrich and R. Ziessel, 2-(2′-Hydroxyphenyl)benzimidazole and 9,10-Phenanthroimidazole Chelates and Borate Complexes: Solution- and Solid-State Emitters, Org. lett. 15(12) (2013) 2918-2921.
[6] A. Malakar, M. Kumar, A. Reddy, H.T. Biswal, B.B. Mandal and G. Krishnamoorthy, Aggregation induced enhanced emission of 2-(2′-hydroxyphenyl)benzimidazole, Photochem. Photobiol. Sci. 15(7) (2016) 937-948.
[7] V. S. Padalkar, P. Ramasami and N. Sekar, A combined experimental and DFT-TDDFT study of the excited-state intramolecular proton transfer (ESIPT) of 2-(2′-hydroxyphenyl) imidazole derivatives, J. fluoresc. 23(5) (2013) 839-851.
[8] S. Park, J. E. Kwon and S. Y. Park, Strategic emission color tuning of highly fluorescent imidazole-based excited-state intramolecular proton transfer molecules, Phys.Chem.Chem.Phys. 14(25) (2012) 8878-8884.
[9] V. S. Padalkar, P. Ramasami and N. Sekar, A comprehensive spectroscopic and computational investigation of intramolecular proton transfer in the excited states of 2-(2′-hydroxyphenyl) benzoxazole and its derivatives, J. Luminesc. 146 (2014) 527-538.
[10] L. Xu, Q. Wang and Y.Zhang, Electronic effect on the photophysical properties of 2-(2-hydroxyphenyl)benzothiazole-based excited state intramolecular proton transfer fluorophores synthesized by sonogashira-coupling reaction, Dyes and Pigments 136 (2017) 732-741.
[11] J. Cheng, D. Liu, W. Li, L. Bao and K. Han, Comprehensive Studies on Excited-State Proton Transfer of a Series of 2-(2′-Hydroxyphenyl)benzothiazole Derivatives: Synthesis, Optical Properties, and Theoretical Calculations, J.Phys.Chem. C 119(8) 2015 4242-4251.
[12] D. Yao, S. Zhao, J. Guo, Z. Zhang, H. Zhang, Y. Liu and Y. Wang, Hydroxyphenyl-benzothiazole based full color organic emitting materials generated by facile molecular modification, J. Mater. Chem. 21(11) (2011) 3568-3570.
[13] M.R.Rao, C.-W.Liao, W.-L.Su and S.-S. Sun, Quinoxaline based D–A–D molecules: high contrast reversible solid-state mechano- and thermo-responsive fluorescent materials, J.Mater.Chem. C 35 (2013) 1 5491-5501.
[14] J. Mei, N. L. C. Leung, R. T. K. Kwok, J. W. Y. Lam, B.-Z. Tang, Aggregation-Induced Emission: Together We Shine, United We Soar!, Chem. Rev. 115 (2015) 11718–11940.
[15] F. Würthner Aggregation-Induced Emission (AIE): A Historical Perspective. Angew. Chem. Int. Ed., *59* (2020) 14192-14196.
[16] Y. Hong, J. W. Y. Lam, Tang, B.-Z. Tang, Aggregation-induced emission, Chem. Soc. Rev., 40 (2011) 5361–5388.
[17] A.J. Stasyuk, P.Bultinck, D.T.Gryko, M.K. Cyrański, The effect of hydrogen bond strength on emission properties in 2-(2'-hydroxyphenyl)imidazo[1,2-a]pyridines, J.Photochem.Photobiol. A 314 (2016) 198-213.
[18] K. Kungwan, F. Plasser, A. J. Aquino, M. Barbatti, P. Wolschann and H. Lischka, The effect of hydrogen bonding on the excited-state proton transfer in 2-(2′-hydroxyphenyl)benzothiazole: a TDDFT molecular dynamics study, Phys. Chem. Chem. Phys. 14(25) (2012) 9016-9025.
[19] A. Douhal, F. Amat-Guerri and A. U. Acuña, Photoinduced Intramolecular Proton Transfer and Charge Redistribution in Imidazopyridines, J. Phys. Chem. 99 (1995) 76-80.

[20] A. Douhal, F. Amat-Guerri and A. U. Acuña, Probing nanocavities with proton-transfer fluorescence, Angew. Chem. Int. Ed. 36 (1997) 1514-1516.
[21] T. Mutai. H. Tomoda, T. Ohkawa, Y. Yabe and K. Araki, Switching of polymorph-dependent ESIPT luminescence of an imidazo[1,2-a]pyridine derivative, Angew. Chem. Int. Ed. 47 (2008) 9522-9524.
[22] T. Mutai, H. Sawatani, T. Shida, H. Shono and K. Araki, Tuning of excited-state intramolecular proton transfer (ESIPT) fluorescence of imidazo[1,2-a]pyridine in rigid matrices by substitution effect, J.Org.Chem., 78 (2013) 2482-2489.
[23] T. Mutai, H. Shono, Y. Shigemitsu and K. Araki, Three-color polymorph-dependent luminescence: crystallographic analysis and theoretical study on excited-state intramolecular proton transfer (ESIPT) luminescence of cyano-substituted imidazo[1,2-a]pyridine, Csyst. Eng. Comm., 16 (2014) 3890-3895.
[24] Y. Shigemitsu, T. Mutai, H. Houjou and K. Araki, Excited-State Intramolecular Proton Transfer (ESIPT) Emission of Hydroxyphenylimidazopyridine: Computational Study on Enhanced and Polymorph-Dependent Luminescence in the Solid State, J.Phys.Chem.A, 116 (2012) 12041-12048.
[25] Y .Shigemitsu, T. Mutai, H. Houjou and K. Araki, Influence of intermolecular interactions on solid state luminescence of imidazopyridines: theoretical interpretations using FMO-TDDFT and ONIOM approaches, Phys.Chem.Chem.Phys. 16 (2014) 14388-14395.
[26] T.Shida, T.Mutai and K.Araki, Sterically induced polymorphism: ON–OFF control of excited-state intramolecular proton transfer (ESIPT) luminescence of 1-methyl-2-(2′-hydroxyphenyl)benzimidazole, Csyst. Eng. Comm. 15 (2013) 10179-10182.
[27] Y.Chi, B. Tong, P.-T.Chou, Metal Complexes with Pyridyl Azolates: Design, Preparation and Applications Coord.Chem.Rev., 2014,281,1-25.
[28] F.-Y.Meng, Y.-H. Hsu, Z.Zhang, P.-J. Wu, Y.-T. Chen, Y.-A. Chen, C.-L. Cheng, C.-M. Chao, K.-M. Liu, P.-T. Chou, The Quest of Excited-State Intramolecular Proton Transfer via Eight-Membered Ring π-Conjugated Hydrogen Bonding System, Chem. Asian. J. 12 (2017) 3010-3015.
[29] T.Arai, M.Moriyama, K.Tokumaru, Novel photoinduced hydrogen atom transfer through intramolecular hydrogen bonding coupled with cis-trans isomerization in cis-1-(2-pyrrolyl)-2-(2-quinolyl)ethane, J.Am.Chem.Soc. 116 (1994) 3171-3172.
[30] K.-Y. Chen, Y.-M. Cheng, C.-H. Lai, C.-C. Hsu, M.-L. Ho, G.-H. Lee, P.-T. Chou, Ortho Green Fluorescence Protein Synthetic Chromophore; Excited-State Intramolecular Proton Transfer via a Seven-Membered-Ring Hydrogen-Bonding System,
J.Am.Chem.Soc. 1209 (2007) 4534-4535.
[31] Y.-H. Hsu, Y.-A. Chen, H.-W.Tseng, Z.Zhang, J.-Y. Shen, W.-T. Chuang, T.-C. Lin, C-S. Lee, W.-Y. Hung, B.-C. Hong, S.-H. Liu, P.-T. Chou, Locked ortho- and para-Core Chromophores of Green Fluorescent Protein; Dramatic Emission Enhancement via Structural Constraint, J.Am.Chem.Soc. 136 (2014) 11805-11812.
[32] V. S. Padalkar and S. Seki, Excited-state intramolecular proton-transfer (ESIPT)-inspired solid state emitters, Chem. Soc. Rev. 45(1) (2016) 169-202.
[33] A. J. Stasyuk, P. J. Cywiński and D. T. Gryko, Excited-state intramolecular proton transfer in 2′-(2′-hydroxyphenyl)imidazo[1,2-a]pyridinesJ. Photochem. Photobiol. C 28 (2016) 116-137.
[34] A.D.Laurent, Y.Houari, P.H.P.R.Carvalho, B.A.D.Neto, D.Jacquemin, ESIPT or not ESIPT? Revisiting recent results on 2,1,3-benzothiadiazole under the TD-DFT light, RSC Advances 4 (2014) 14189-14192.
[35] C.Zarias, S.Budzak, A.D.Laurent, G.Ulrich, D.Jacquemin, Tuning ESIPT fluorophores into dual emitters, Chem.Sci., 7 (2016) 3763-3774.
[36] O. Louant, B. Champagne and V. Liégeois, Investigation of the Electronic Excited-State Equilibrium Geometries of Three Molecules Undergoing ESIPT: A RI-CC2 and TDDFT Study, J. Phys. Chem. A 122(4) 2018 972-984.
[37] A. L. Sobolewski, W. Domcke, Efficient Excited-State Deactivation in Organic Chromophores and Biologically Relevant Molecules: Role of Electron and Proton Transfer Processes, in: W. Domcke, D.R.Yarkony,H.Koppel (Eds.), Conical Intersections: Theory, Computation and Experiment, World Scientific Pub Co Inc, 2011, pp. 51-82.
[38] J. Jankowska, M. F. Rode, J. Sadlej and A. L. Sobolewski, Excited-state intramolecular proton transfer: photoswitching in salicylidene methylamine derivatives, Chem. Phys. Chem. 15(8) (2012) 1643-1652.
[39] H. Lischka, D. Nachtigallová, A. J. Aquino, P. G. Szalay, F. Plasser, F. B. Machado and M. Barbatti, Multireference Approaches for Excited States of Molecules, Chem. Rev. 118(15) (2018) 7293-7361.
[40] M. Barbatti, A. J. Aquino, H. Lischka, C. Schriever, S. Lochbrunner and E. Riedle, Ultrafast internal conversion pathway and mechanism in 2-(2′-hydroxyphenyl) benzothiazole: a case study for excited-state intramolecular proton transfer systems, Phys. Chem. Chem. Phys., 11(9) (2009) 1406-1415.
[41] M. Dommett and R. Crespo-Otero. Excited state proton transfer in 2′-hydroxychalcone derivatives, Phys.

Chem. Chem.Phys. 19(3) (2017) 2409-2416.
[42] M. Dommett, R. Miguel and R. Crespo-Otero, How Inter- and Intramolecular Processes Dictate Aggregation-Induced Emission in Crystals Undergoing Excited-State Proton Transfer, J. Phys. Chem. Lett. 8(24) (2017) 6148-6153.
[43] R.Omidyan and M.Iravani, Excited-state intramolecular proton transfer and photoswitching in hydroxyphenyl-imidazopyridine derivatives: A theoretical study, J.Chem.Phys, 145 (2016) 184303.
[44] R.Omidyan and M.Iravani, Excited State Proton Transfer and Deactivation Mechanism of 2-(4′-Amino-2′-hydroxyphenyl)-1H-imidazo-[4,5-c]pyridine and Its Analogues: A Theoretical Study, J.Phys.Chem.A 120 (2016) 1012-1019.
[45] J. Mei, N. L. Leung, R. T. Kwok, J. W. Lam and B. Z. Tang, Aggregation-Induced Emission: Together We Shine, United We Soar, Chem. Rev. 115(21) (2015) 11718-11940.
[46] Q. Peng, Y. Yi, Z. Shuai and J. Shao, Toward Quantitative Prediction of Molecular Fluorescence Quantum Efficiency: Role of Duschinsky Rotation, J. Am. Chem. Soc. 19(30) (2007) 9333-9339.
[47] Q. Wu, Q. Peng, Y. Niu, X. Gao and Z. Shuai, Theoretical Insights into the Aggregation-Induced Emission by Hydrogen Bonding: A QM/MM Study, J. Phys. Chem. A 116(15) (2012) 3881-3888.
[48] L. Lin, J. Fan, L. Cai and C. K. Wang, Theoretical perspective of the excited state intramolecular proton transfer for a compound with aggregation induced emission in the solid phase, RSC Advances, 70 (2017) 44089-44096.
[49] J. Fan, L. Lin and C. K. Wang, Excited state properties of non-doped thermally activated delayed fluorescence emitters with aggregation-induced emission: a QM/MM study, J. Mater. Chem. C 33 (2017) 8390-8399.
[50] X.-L. Peng, S. Ruis-Barragan, Z.-S. Li, Q.-S. Li, L.Blancafort, Restricted access to a conical intersection to explain aggregation induced emission in dimethyl tetraphenylsilole, J.Mater.Chem. C 4 (2016) 2802-2810.
[51] Q. Li, L. Blancafort, A conical intersection model to explain aggregation induced emission in diphenyl dibenzofulvene, Chem.Comm., 49 (2013) 5966-5968.
[52] T.Mutai, T.Muramatsu, I.Yoshikawa, H.Houjou and M.Ogura, Development of Imidazo[1,2-a]pyridine Derivatives with an Intramolecular Hydrogen-Bonded Seven-Membered Ring Exhibiting Bright ESIPT Luminescence in the Solid State, Org.Lett.. 21(7) (2019) 2143-2146.
[53] TURBOMOLE V7.0 2015, a development of University of Karlsruhe and Forschungszentrum Karlsruhe GmbH, 1989-2007, TURBOMOLE GmbH, since 2007; available from http://www.turbomole.com.
[54] MOLPRO, version 2015.1, a package of *ab initio* programs, H.-J. Werner, P. J. Knowles, G. Knizia, F. R. Manby, M. Schütz, and others, http://www.molpro.net.
[55] F. Aquilante, L. De Vico, N. Ferré, G. Ghigo, P.-Å. Malmqvist, P. Neogrády, T.B. Pedersen, M. Pitonak, M. Reiher, B.O. Roos, L. Serrano-Andrés, M. Urban, V. Veryazov, R. Lindh, MOLCAS 7: the next generation, *J. Comp.Chem.* 31 (2010) 224-247.
[56] OpenMolcas, https://gitlab.com/Molcas/OpenMolcas.
[57] M. Barbatti, M. Ruckenbauer, F. Plasser., J. Pittner, G. Granucci, M. Persico and H. Lischka, Newton-X: a surface-hopping program for nonadiabatic molecular dynamics, Wiley Interdisciplinary Reviews: Computational Molecular Science 4(1) (2014) 26-33.
[58] J. Kruszewski, T.M. Krygowski, Definition of aromaticity basing on the harmonic oscillator model, Tetrahedron Lett. 13 (1972) 3839-3842.
[59] T. M. Krygowski, Crystallographic studies of inter- and intramolecular interactions reflected in aromatic character of .pi.-electron systems, J.Chem.Inf.Comput.Sci. 33(1) (1993) 70-78.
[60] A. J. Stayuk, M. Banasiewicz, M. K. Cyrański, D. T. Gryko, Imidazo[1,2-a]pyridines Susceptible to Excited State Intramolecular Proton Transfer: One-Pot Synthesis via an Ortoleva–King Reaction, J.Org.Chem. 77 (2012) 5552-5558.

Table 1 Key geometrical parameter of 8(PhOH)-IP, 8(ThOH)-IP and 8(F-PhOH)-IP in the ground states. Bond length (Å), dihedral angle (degree) optimized by different levels of theories.

	B3LYP		RI-ADC(2)		RI-CC2		Expl.
	SVP	TZVP	SVP	TZVP	SVP	TZVP	
8(PhOH)-IP							
r_{ON}	2.62	2.66	2.69	2.67	2.66	2.66	2.66
ϕ	35.64	38.16	43.86	41.53	40.43	40.46	40.58
8(ThOH)-IP							
r_{ON}	2.58	2.60	2.65	2.63	2.63	2.61	2.56
ϕ	0.12	0.19	26.61	21.14	22.40	17.45	3.32
8(F-PhOH)-IP							
r_{ON}	2.62	2.67	2.69	2.68	2.67	2.66	3.07
ϕ	38.85	42.15	45.55	44.74	44.44	43.74	57.58

Table 2 Quasi-HOMA indexes of the three compounds. The HOMA parameters are from reference [55].

	8PhOH-IP	**8ThOH-IP**	**8-F-PhOH-IP (in-plane)**	**8-F-PhOH-IP (out-of-plane)**	**H-1,2-HPIP**	**F-1,2-HPIP**	**CN-1,2-HPIP**	**Me-1,2-HPIP**
Quasi- HOMA	0.319	0.559	0.319	0.308	0.400[(a)]	0.396[(a)]	0.426[(a)]	0.404[(a)]

(a)Reference [14]

Table 3 The lowest transition energies of 8(PhOH)-IP

		TDDFT(B3LYP)		RI-ADC(2)		RI-CC2		CASPT2	Expl.
state		SVP	TZVP	SVP	TZVP	SVP	TZVP		
S_0-enol	S_0->S_1								3.79 (Cycl.)
	(in vacuo)	3.47	3.57	4.14	4.00	4.14	3.98	4.06[(b)]	
	(solvent)	3.55	3.64	4.18	4.03	4.20	4.04	4.06[(b)]	
S_1-enol	S_1->S_0								3.32 (Cylc.)
	(in vacuo)	2.95[(b)]	2.91[(b)]	3.33[(a)]	3.19	3.24[(b)]	3.11	3.10[(b)]	No emission (solid)
	(solvent)	2.99[(b)]	2.94[(b)]	3.41[(a)]	3.21	3.33[(b)]	3.18	3.37[(b)]	
S_1-keto	S_1->S_0	(c)							2.11 (Cycl.)
	(in vacuo)		0.16	1.46	1.52	1.63	1.68	1.89[(b)]	2.35 (solid)
	(solvent)		0.79	1.64	1.65	1.78	2.08	2.10[(b)]	

(a) singlepoint calculations using ADC(2)/TZVP optimized geometries

(b) singlepoint calculations using CC2/TZVP optimized geometries

(c) SCF not converged because of the instability near the S_0/S_1 conical intersection

(solvent) COSMO model for RI-ADC(2) and RI-CC2. PCM for CASPT2

(Cycl.) measured in cyclohexane in reference [49]

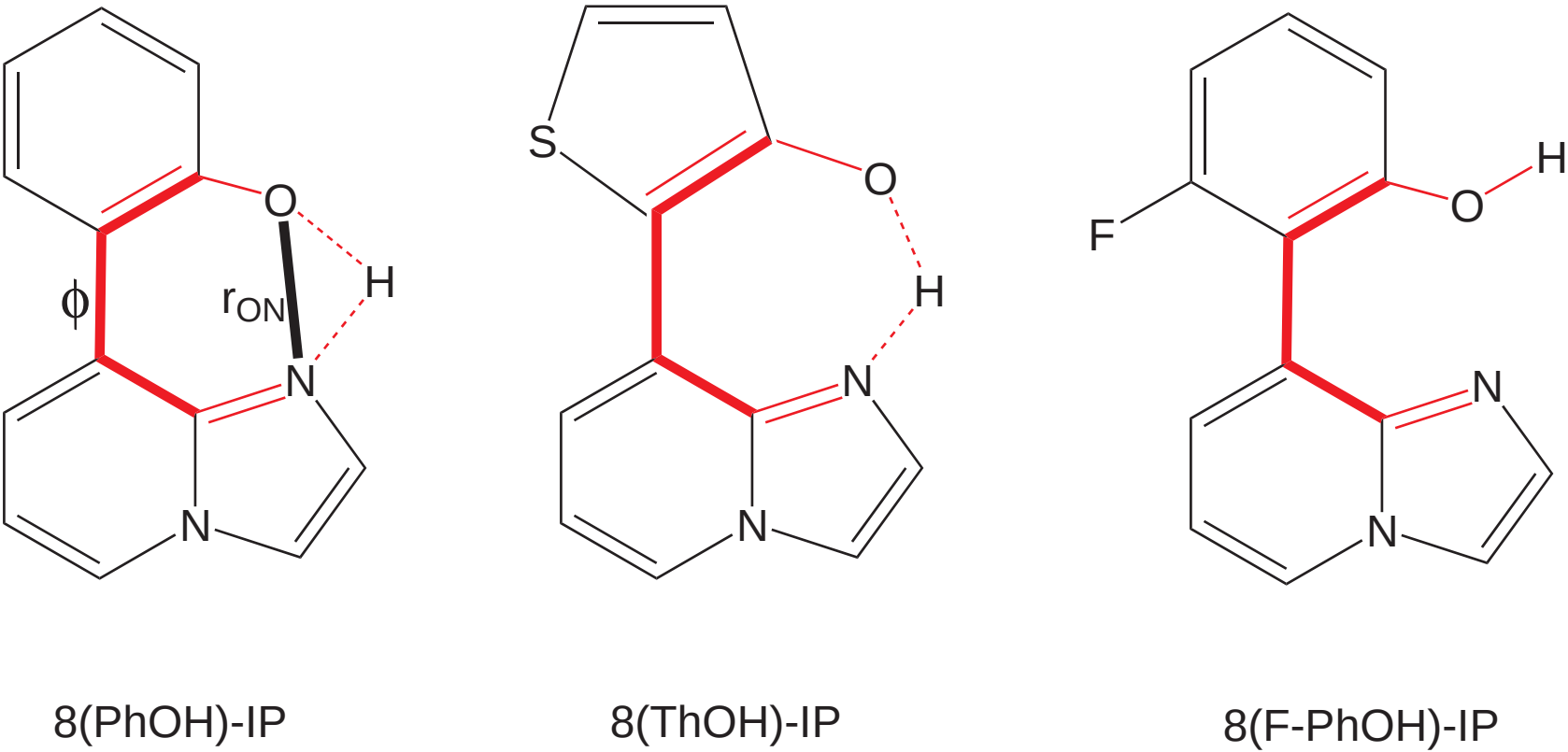

Fig. 1. The seven-memberd ESIPT molecules : 8(PhOH)-IP, 8(ThOH)-IP and 8(F-PhOH)-IP

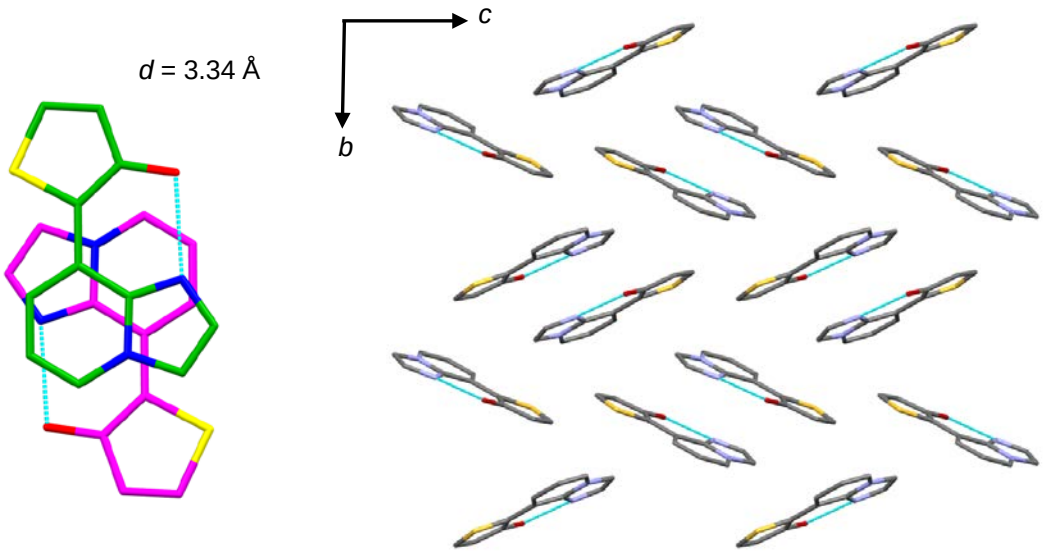

Fig. 2. Molecular packing of **2** in crystal obtained by X-ray crystallographic analysis. The intramolecular hydrogen bond is indicated as a light-blue dotted line. The distance between the stacked IP rings was 3.34 Å. (Reprinted with permission from ref. 49 Copyright 2019 American Chemical Society.)

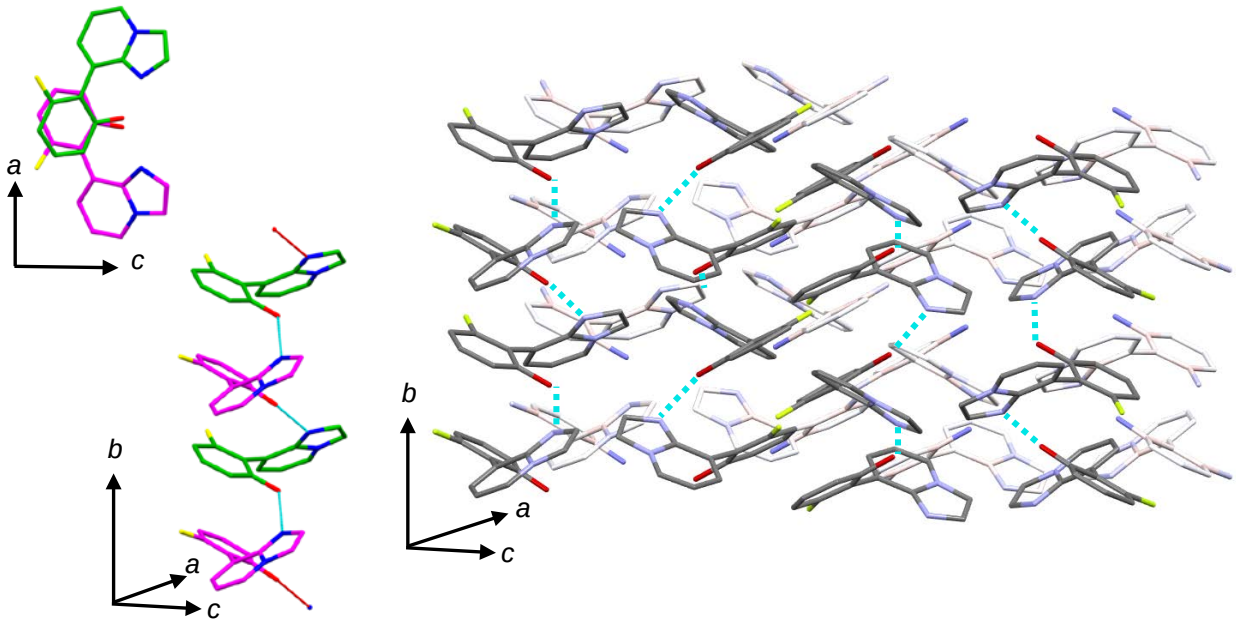

Fig. 3. Molecular packing of **3** in crystal obtained by X-ray crystallographic analysis. The intermolecular hydrogen bond is indicated as a light-blue dotted line. . (Reprinted with permission from ref. 49 Copyright 2019 American Chemical Society.)

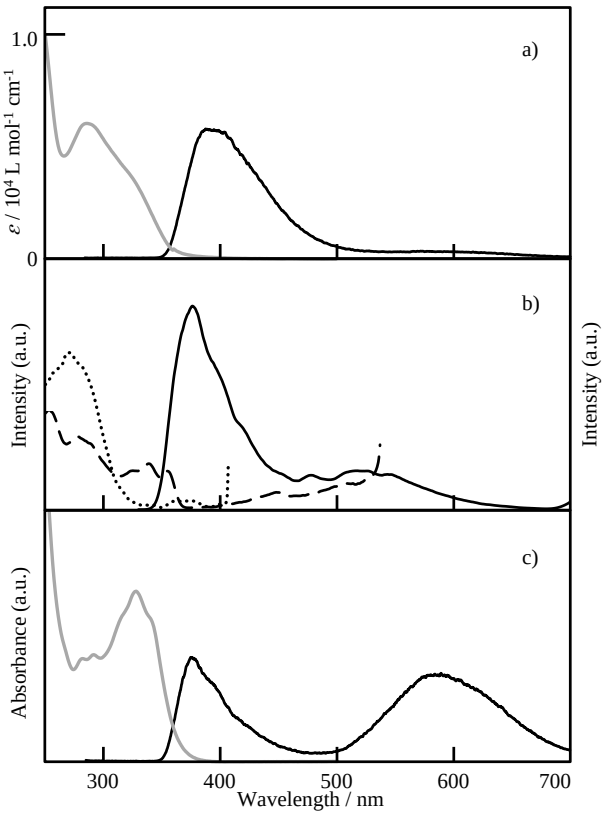

Fig. 4. Absorption (gray), fluorescence (solid) and excitation (dotted and dashed) spectra of 8(PhOH)-IP. a) MeTHF solution at room temperature, b) frozen MeTHF solution in 77 K, excitation spectra were monitored at 420 (dotted) and 550 (dashed) nm, and c), cyclohexane solution at room temperature. . (Reprinted with permission from ref. 49 Copyright 2019 American Chemical Society.)

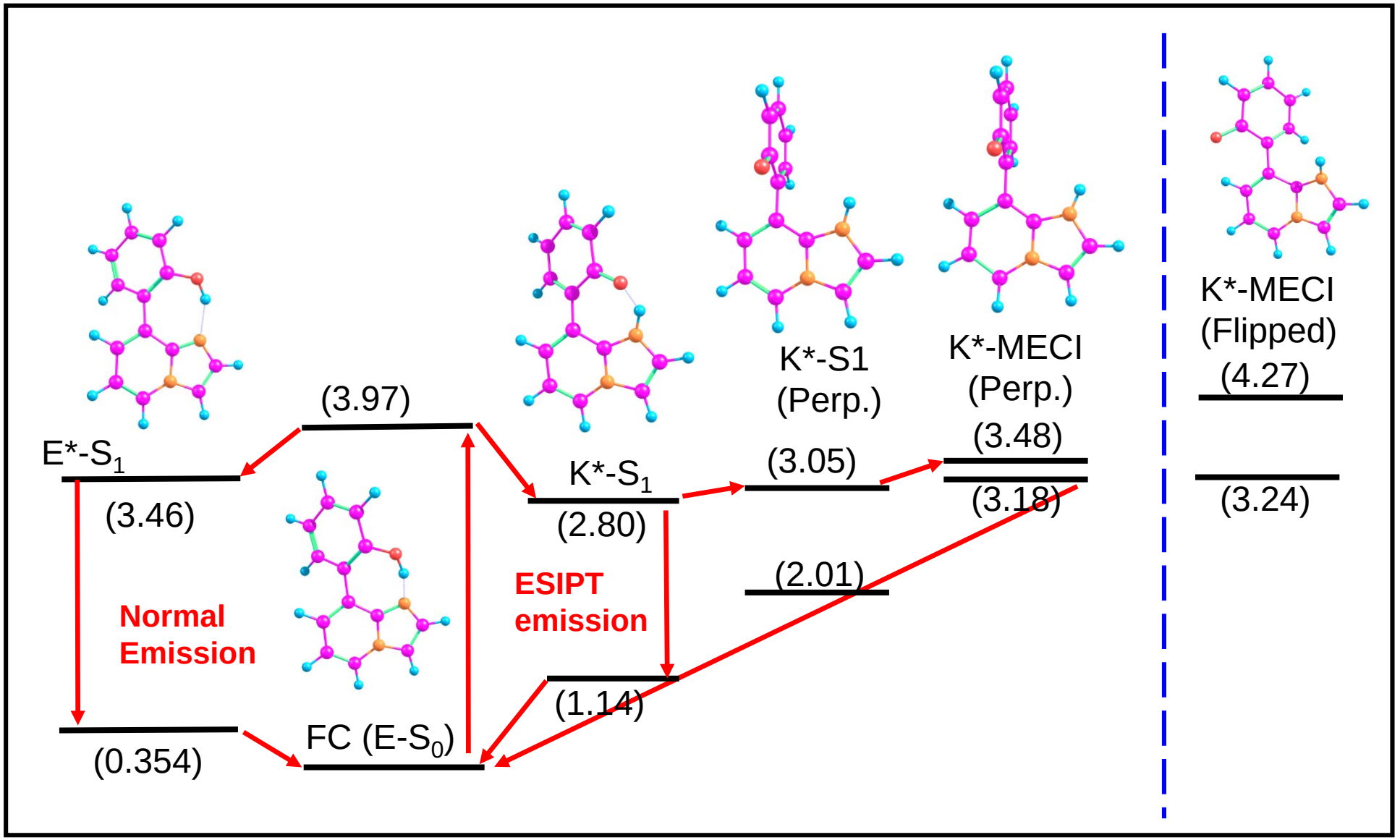

Fig. 5. The schematic energy diagram of 8(PhOH)-IP calculated at RI-CC2/TZVP level of theory. (energies in eV relative to E-S_0)

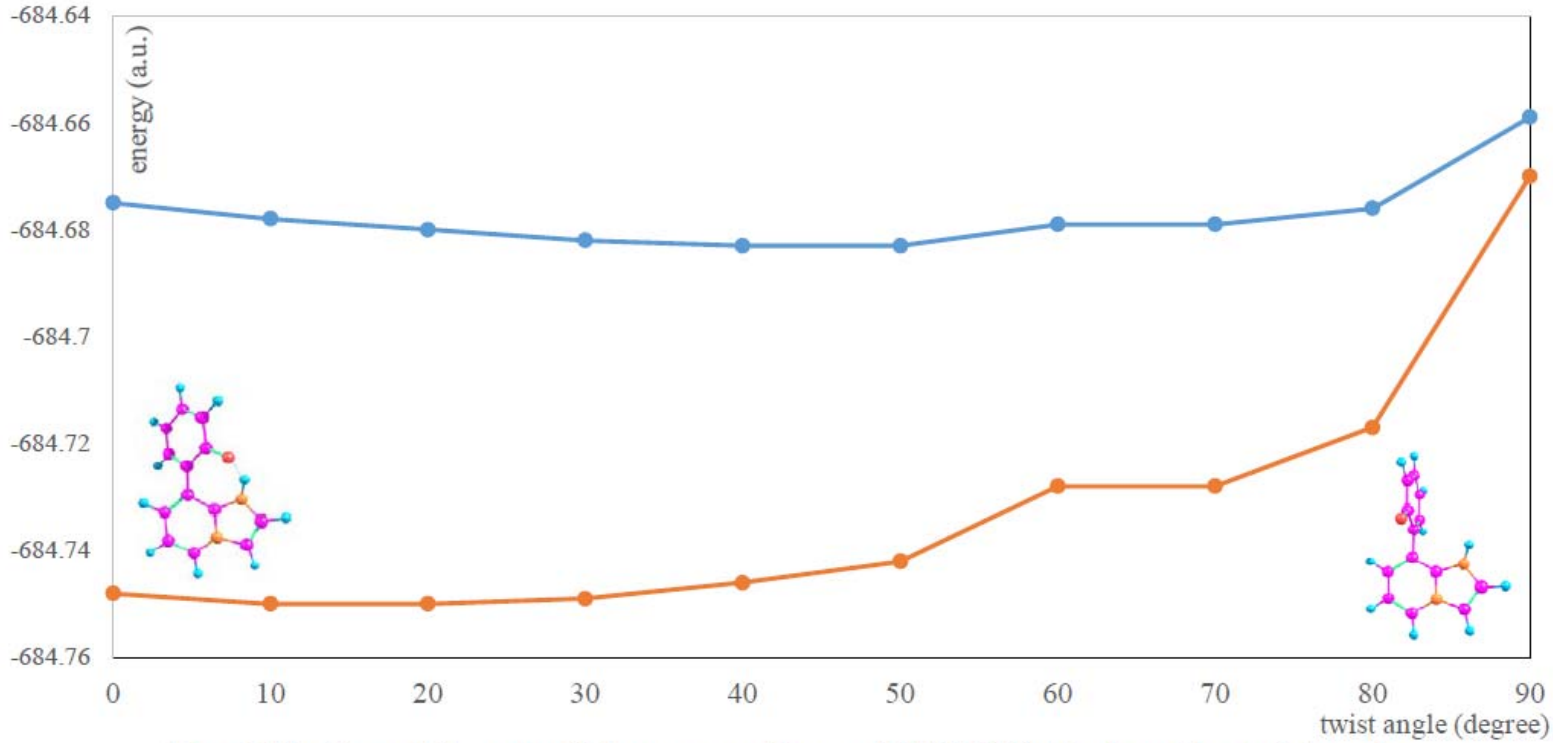

Fig. 6 The S_0 and S_1 potential enegy surfaces of 8(PhOH)-IP along the twist angle.

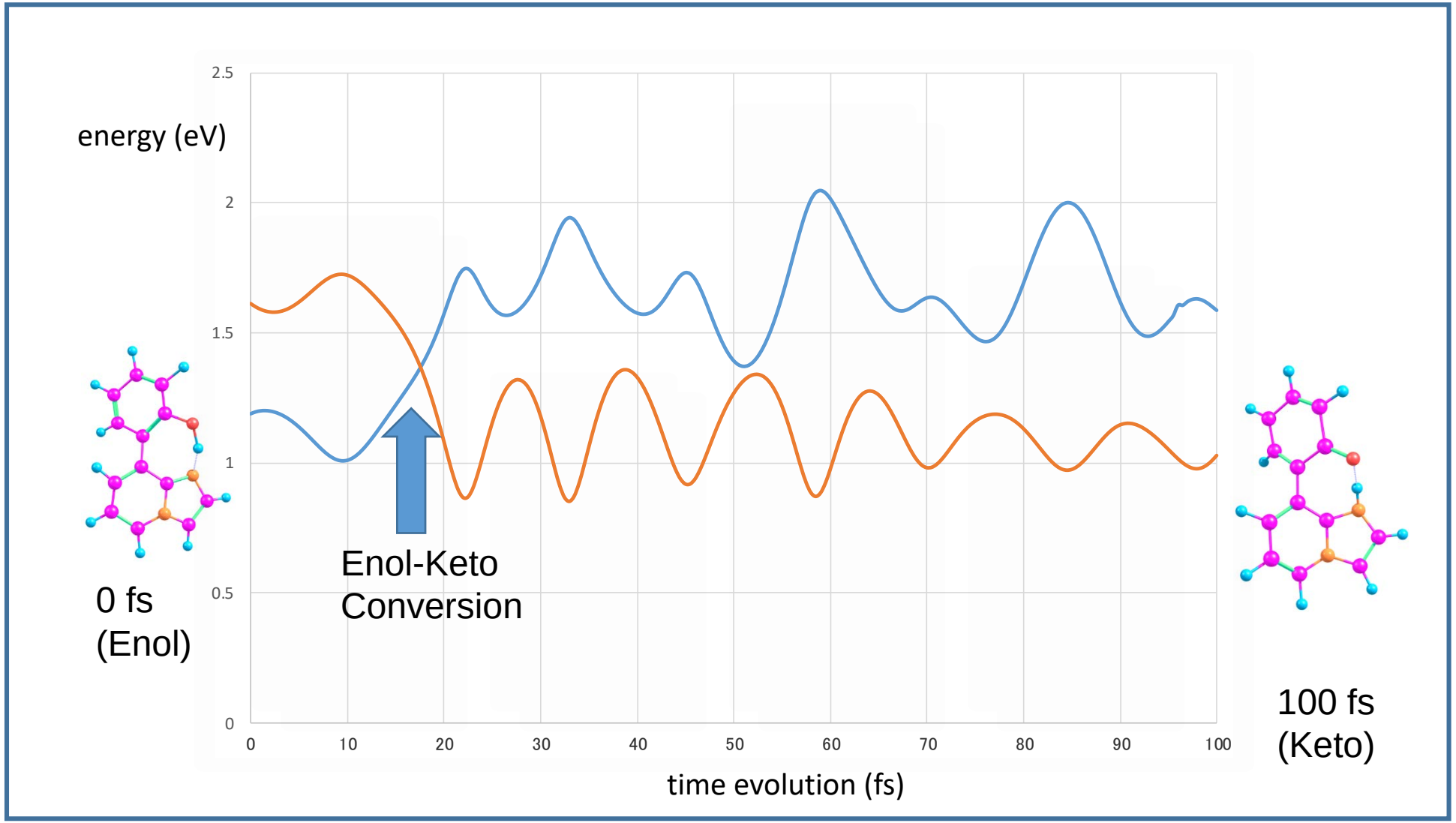

Fig. 7 The time evolution of S_0-S_1 gap associated with ESIPT trajectory of 8(PhOH)-IP

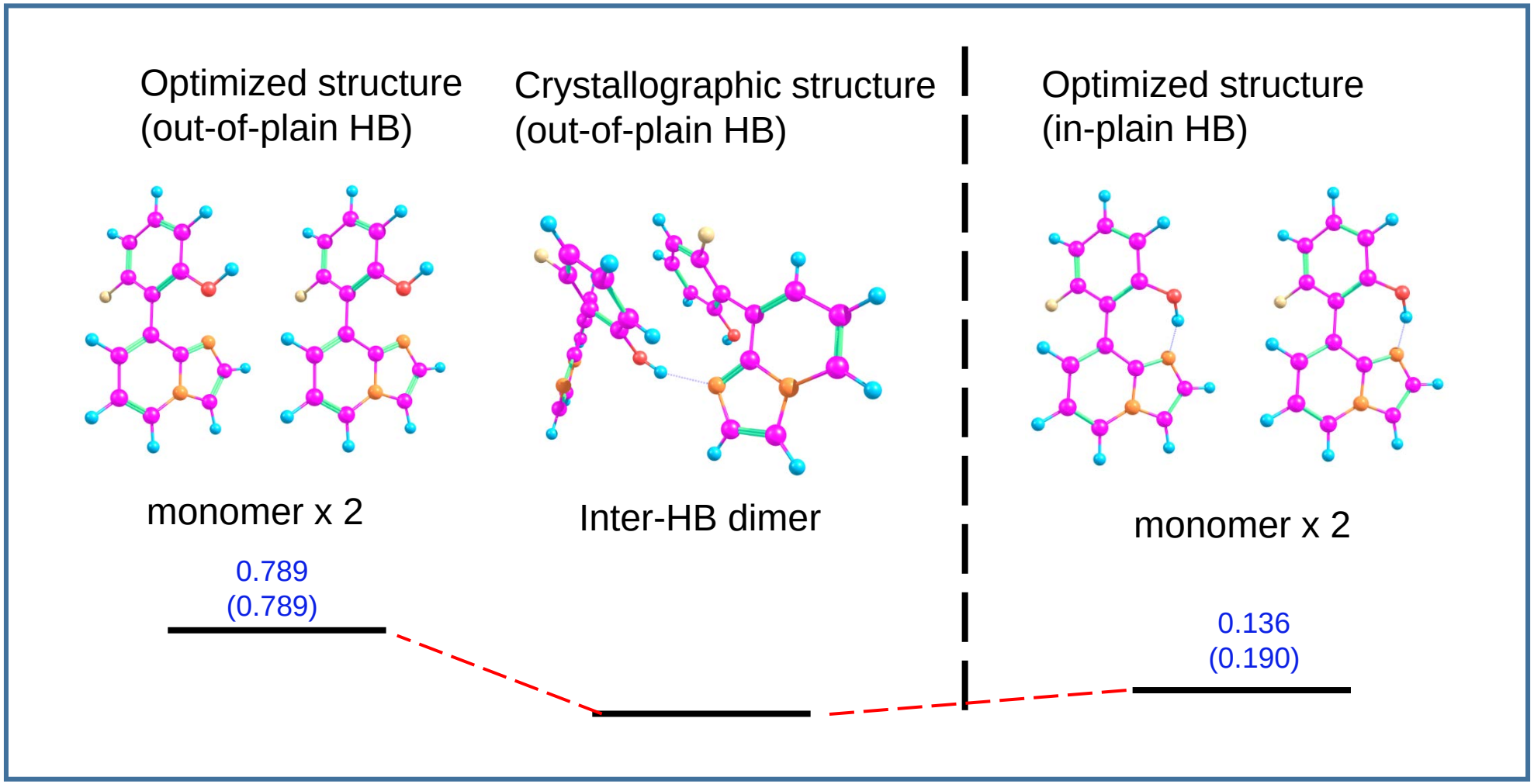

Fig. 8 The Relative energy diagram of 8(F-PhOH)-IP calculated at RI-CC2/ TZVP and RI-CCSD(T)/TZVP (*in parenthesis*) level of theory.
The energies are in eV relative to the crystallographic structure (out-of-plain HB)

Table S1 Key geometrical parameter of 8(PhOH)-IP, 8(ThOH)-IP and 8(F-PhOH)-IP of S_1-enol form.

Bond length (Å), dihedral angle (degree) optimized by different level of theory.

	B3LYP		RI-ADC(2)		RI-CC2	
	SVP	TZVP	SVP	TZVP	SVP	TZVP
8(PhOH)-IP						
r_{ON}	(*)	(*)	(*)	2.48	(*)	2.44
ϕ	(*)	(*)	(*)	23.36	(*)	25.43
8(ThOH)-IP						
r_{ON}	2.55	2.57	2.48	2.48	2.53	2.49
ϕ	27.18	28.18	34.40	11.36	10.59	13.80
8(F-PhOH)-IP						
r_{ON}	(*)	(*)	(*)	2.68	(*)	(*)
ϕ	(*)	(*)	(*)	37.79	(*)	(*)

(*) not found. Slipped into the S_1-keto form.

Table S2 Key geometrical parameter of 8(PhOH)-IP, 8(ThOH)-IP and 8(F-PhOH)-IP of S_1-keto form.

Bond length (Å), dihedral angle (degree) optimized at different levels of theory.

	B3LYP		RI-ADC(2)		RI-CC2	
	SVP	TZVP	SVP	TZVP	SVP	TZVP
8(PhOH)-IP						
r_{ON}	(a)	4.07	2.72	2.31	2.72	2.69
ϕ	(a)	86.33	44.79	36.43	47.12	43.19
8(ThOH)-IP						
r_{ON}	2.61	2.64	2.81	2.77	2.82	2.78
ϕ	0.93	21.67	44.54	41.46	47.19	44.02
8(F-PhOH)-IP						
r_{ON}	3.94	3.94	2.73	2.70	2.74	2.72
ϕ	91.63	91.75	45.83	44.11	47.59	45.88

(a) SCF instability near the S_0/S_1 proximity.

Table S3 The lowest transition energies of 8(ThOH)-IP.

		TDDFT(B3LYP)		RI-ADC(2)		RI-CC2		CASPT2	Expl.
state		SVP	TZVP	SVP	TZVP	SVP	TZVP		
S_0-enol	S_0->S_1								3.47 (Cycl.)
	(in vacuo)	3.51	3.46	3.85	3.65	3.84	3.67	3.84[(b)]	
	(solvent)	3.45	3.40	3.85	3.66	3.86	3.66	3.78[(b)]	
S_1-enol	S_1->S_0								3.16 (Cycl.)
	(in vacuo)	3.32	3.28	3.32	3.24	3.53	3.33	3.35[(b)]	No emission (Solid)
	(solvent)	3.30	3.27	3.35	3.20	3.49[)]	3.30	2.93[(b)]	
S_1-keto	S_1->S_0								No emission (Cycl.)
	(in vacuo)	3.52	3.46	2.27	2.66	2.71	2.75	2.69[(b)]	2.63 (Solid)
	(solvent)	3.45	3.40	2.73	2.79	3.05	2.90	2.60[(b)]	

(b) singlepoint calculations using CC2/TZVP optimized geometries

(solvent) COSMO model for RI-ADC(2) and RI-CC2. PCM for CASPT2

(Cycl.) measured in cyclohexane in reference [49]

Table S4 The lowest transition energies of 8(F-PhOH)-IP.

		TDDFT(B3LYP)		RI-ADC(2)		RI-CC2		CASPT2	Expl.
state		SVP	TZVP	SVP	TZVP	SVP	TZVP		
S_0-enol[a]	S_0->S_1								3.92 (MeTHF)
	(in vacuo)	3.61	3.71	4.27	4.11	4.27	4.14	3.52[c]	
	(solvent)	3.69	3.77	4.28	4.11	4.32	4.15	4.11[c]	
S_1-enol[a]	S_1->S_0								3.22 (Cycl.)
	(in vacuo)	3.31[b]	3.22[b]	3.44[b]	3.28	3.56[b]	3.36[b]	3.17[b]	3.22 (solid)
	(solvent)	3.26[b]	3.17[b]	3.18[b]	3.27	3.56[b]	3.38[b]	2.83[b]	
S_1-keto[a]	S_1->S_0								2.07 (Cycl.)
	(in vacuo)	0.055	0.27	1.63	1.63	1.76	1.76	2.15[c]	No emission (solid)
	(solvent)	0.67	0.89	2.60	2.60	2.72	2.71	2.13[c]	

(a) in-plane optimized geometry

(b) Using the ADC(2)/TVP optimized geometry

(c) Using the CC2/TVP optimized geometry

(solvent) COSMO model for RI-ADC(2) and RI-CC2. PCM for CASPT2

(MeTHF) measured in methyltetrahydrofuran in reference [49]

(Cycl.) measured in cyclohexane in reference [49]

Table S5 The Configuration weights [a] (CI coefficients) of 8(PhOH)-IP, 8(ThOH)-IP and 8(F-PhOH)-IP

	8(PhOH)-IP			8(ThOH)-IP		
	S_0-enol	S_1-enol	S_1-keto	S_0-enol	S_1-enol	S_1-keto
Main Weight	0.92	0.78	0.85	0.86	0.70	0.85
configuration	(G.S.)[b]	(H->L)[c]	(H->L)[c]	(G.S.)[c]	(H->L)[c]	(H->L)[c]

	F-8(PhOH)-IP		
	S_0-enol	S_1-enol	S_1-keto
Weight	0.92	0.76	0.74
configuration	(G.S.)	(H->L)	(H->L)

(a) MS-CASPT2(14e,10o)/ANO-L using RI-CC2/TZVP optimized geometries

(b) Ground state configuration

(c) HOMO to LUMO one electron excitation configuration

Table S6 Abbreviation list

DFT :	Density Functional Theory
TDDFT :	Time Dependent Density Functional Theory
MS-CASPT2 :	Multi State Complete Active Space Perturbation Theory (2^{nd} Order)
IPEA :	Ionization Potential Electron Affinity
RI-ADC(2) :	Resolution Identity Algebraic Diagrammatic Construction(2^{nd} Order)
RI-CC2:	Resolution Identity Coupled Cluster (2^{nd} Order)
CCSD(T):	Coupled Cluster Single Double (Effective Triple Correction)
RI-MP2 :	Resolution Identity Møller Plesset (2^{nd} Order)
ESIPT :	Excited-State Intramolecular Proton Transfer
AIE :	Aggregation Induced Emission
HB :	Hydrogen Bond
MECI :	Minimum Energy Conical Intersection
BSSE :	Basis Set Superposition Error
HOMA :	Harmonic Oscillator Model of Aromaticity
COSMO :	Conductor like Screening Model
PCM :	Polarizable Continuum Model

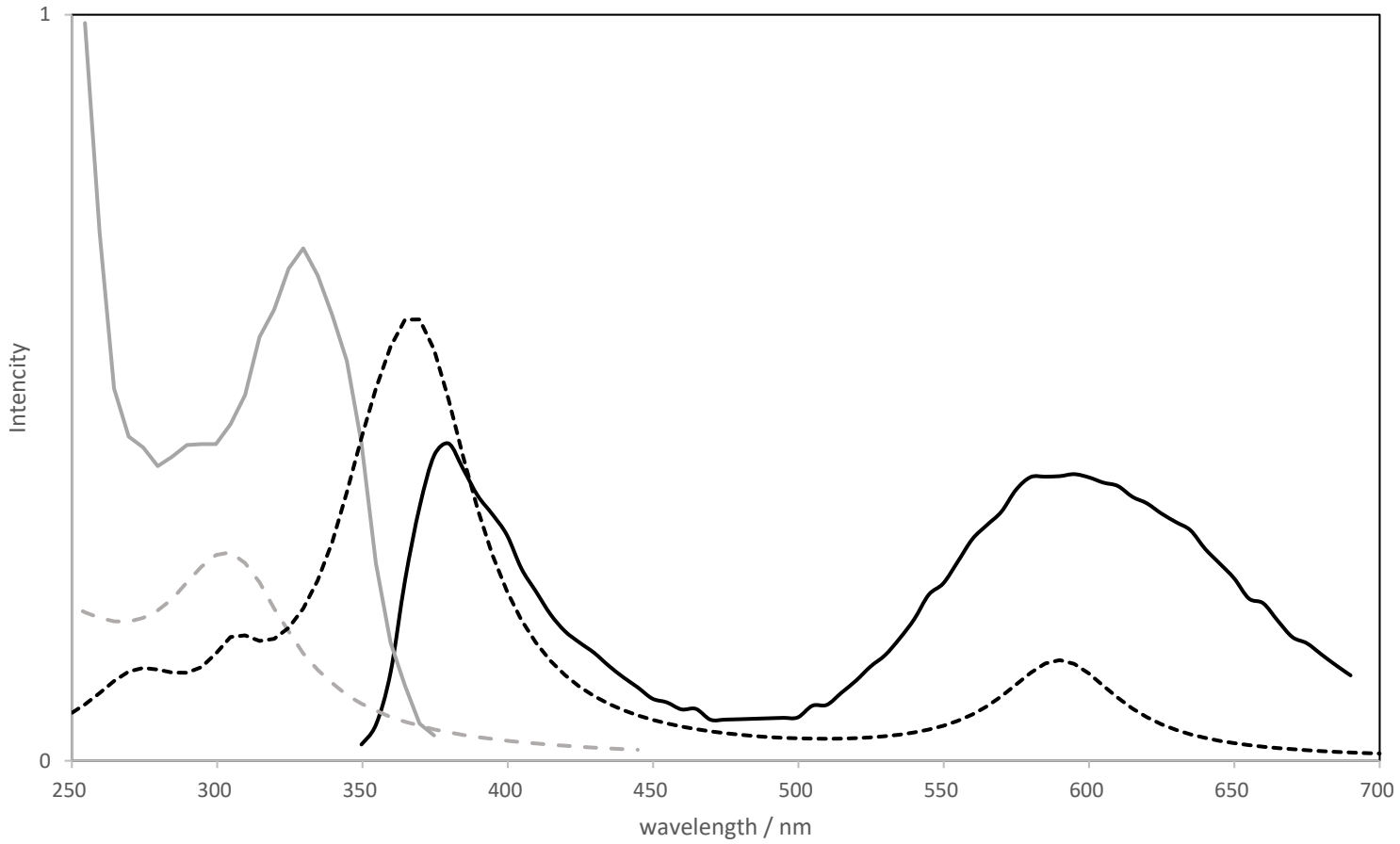

Fig. S1 Experimental and Simulated Spectra of 8(PhOH)-IP in cyclohexane.
Electronic spectra : Experiment (gray solid), Simulation (gray dashed)
Luminescence spectra: Experiment (black solid), Simulation (brack dashed)
Simulation spectra were created by MS-CASPT2/ANO-L.

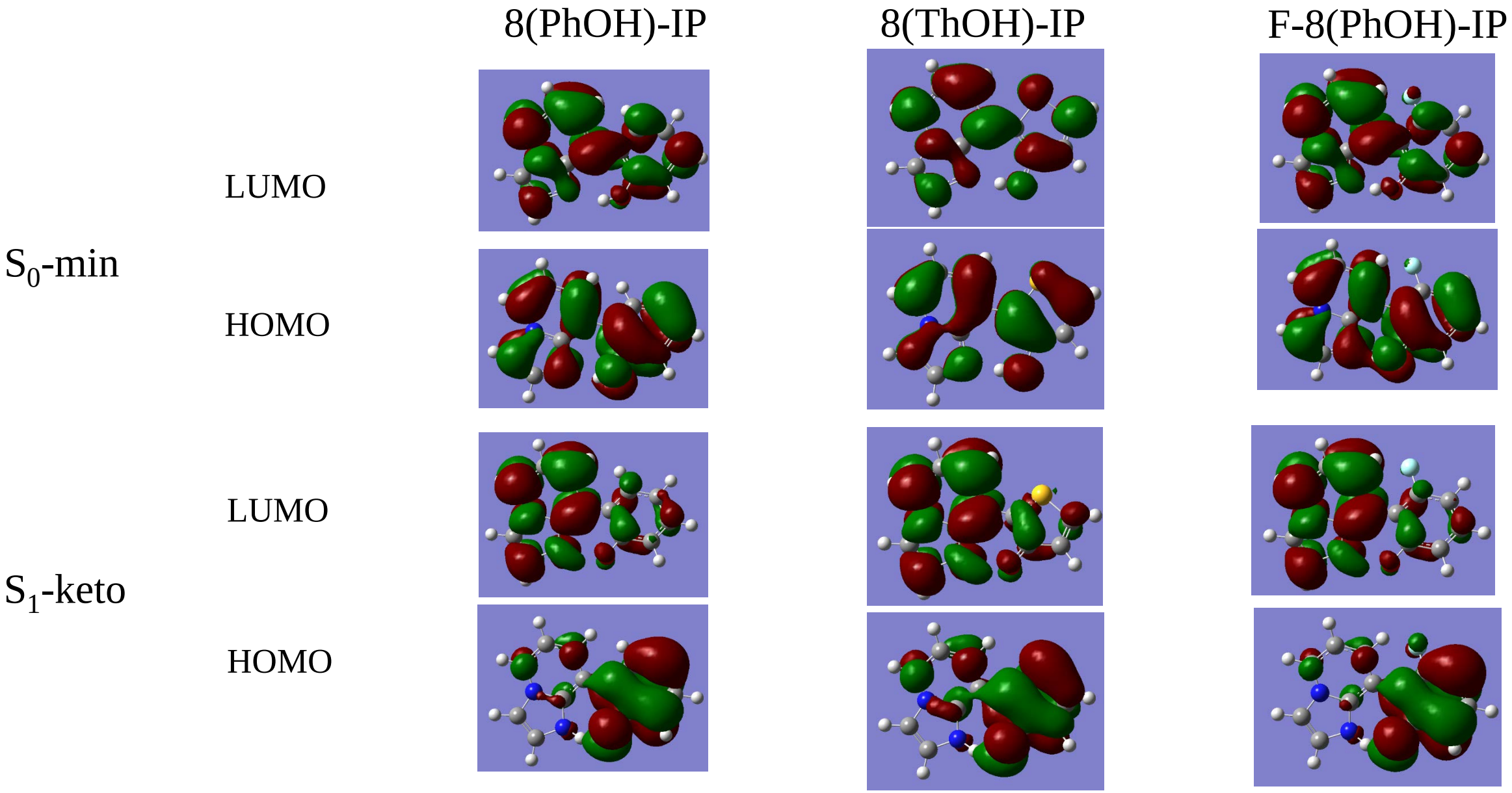

Fig S2 Frontier molecular orbitals in the S_0 and the S_1-keto of 8(PhOH)-IP, 8(ThOH)-IP and F-8(PhOH)-IP computed at CAM-B3LYP/6-31G(d) level.

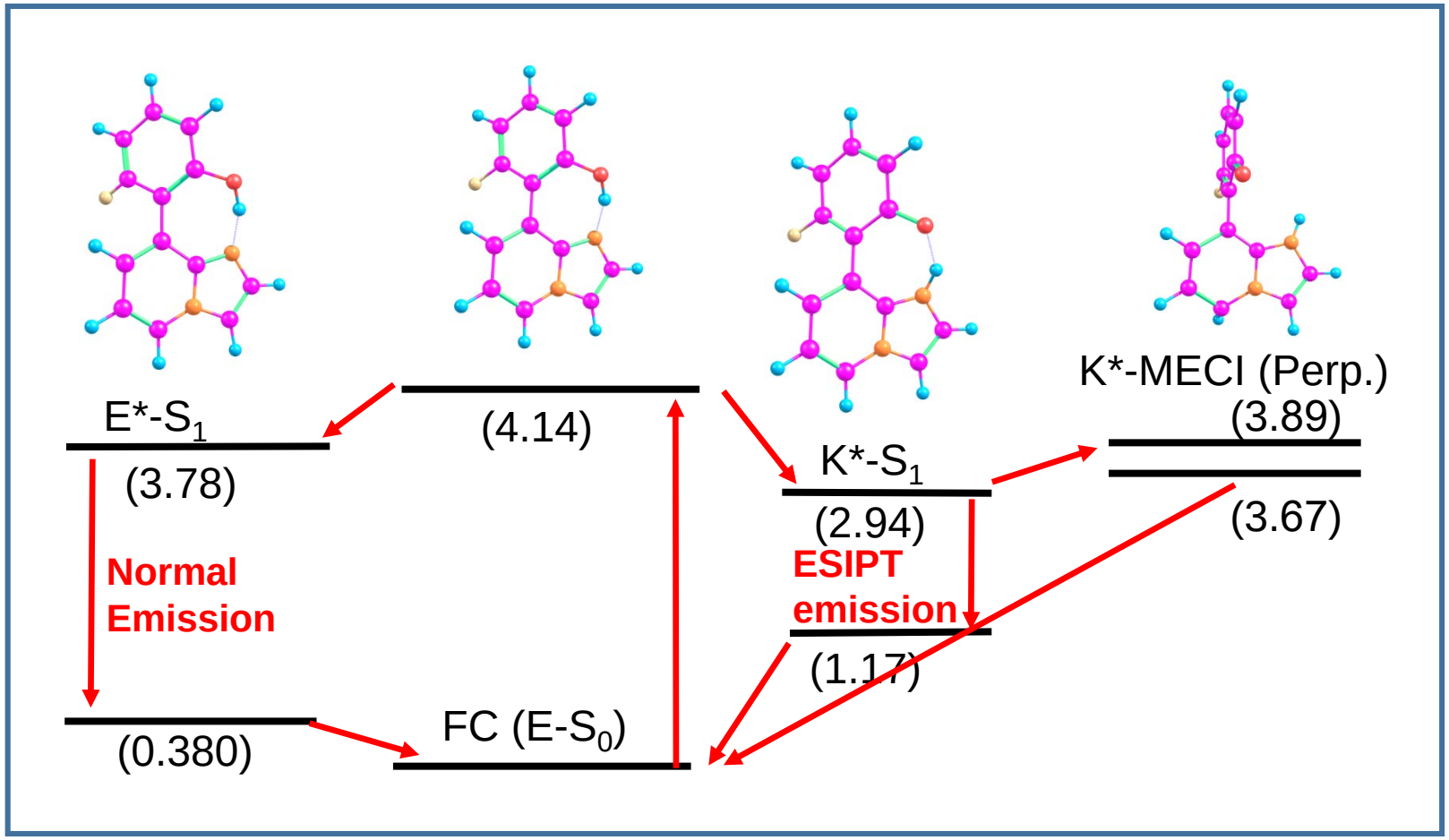

Fig. S3 The energy diagram of 8(F-PhOH)-IP (in-plain form) calculated at RI-CC2/TZVP level of theory.
The energies are in eV relative to E-S_0.

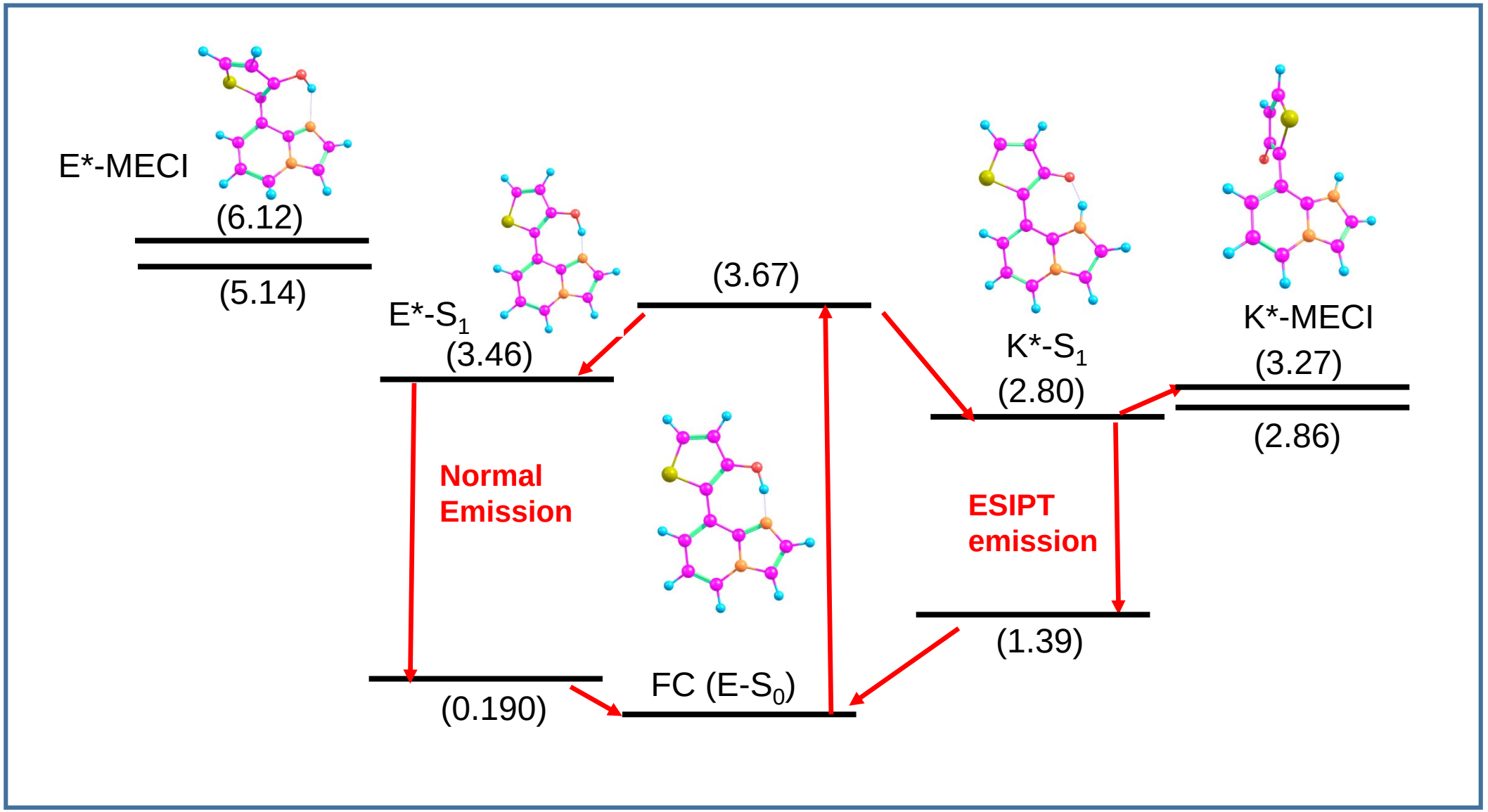

Fig. S4 The energy diagram of 8(ThOH)-IP calculated at RI-CC2/TZVP level of theory. The energies are in eV relative to E-S_0